Correlated fluctuations in the polarization modes of a vertical-cavity semiconductor laser

M. B. Willemsen, M. P. van Exter, and J. P. Woerdman
Huygens Laboratory, Leiden University, P.O. Box 9504, 2300 RA Leiden, The Netherlands
(Received 23 June 1999)

The correlated intensity fluctuations in the two polarization modes (x and y) of a TEM_{00} vertical-cavity semiconductor laser are studied experimentally and theoretically. We show that the dynamics of the laser polarization and total output power are almost completely decoupled, and demonstrate how the frequency dependence of the correlation function C_{xy} is related to dichroism and relaxation oscillations. [S1050-2947(99)08211-6]

PACS number(s): 42.65.Pc, 42.55.Px

I. INTRODUCTION

The vertical-cavity surface-emitting laser (VCSEL) is a novel type of semiconductor laser with an almost circular geometry and a very short cavity. Benefits of this construction are, for example, that the output beam is circular and that lasing occurs in a single longitudinal mode. On the other hand, the almost perfect circular symmetry results in a limited polarization stability, and may even lead to polarization switching [1–3]. This unstable behavior is promoted by the quantum noise, which is relatively strong in a VCSEL, due to its small modal volume. It is well known that the light emitted by VCSEL's is approximately linearly polarized. More detailed studies have shown that the output light consists of a strong lasing mode and a weak nonlasing mode, which is orthogonally linearly polarized with respect to the lasing mode [4]. The relative strength of this nonlasing mode quantifies the polarization fluctuations in the VCSEL.

A proper understanding of polarization fluctuations in VCSEL's is important for practical applications and also for more fundamental topics, like the generation of intensity-squeezed light. In applications, polarization-sensitive elements may lead to the detection of mode-partition noise, resulting in a degradation of the signal-to-noise ratio. For the generation of squeezed light, it is important to know how large the effect of the polarization fluctuations on the total intensity noise is, and whether polarization fluctuations can deteriorate squeezing.

The aim of this paper is to study, experimentally as well as theoretically, the intensity fluctuations of the two polarization modes of a single-transverse-mode TEM_{00} VCSEL, and the correlation between these fluctuations. So far, in most studies of the correlation of a two-polarization-mode laser, the amount of acquired insight was limited [5–7], since the theoretical description was rather complicated and performed numerically. In this paper, we present a direct comparison of experimental data obtained on a VCSEL oscillating in the TEM_{00} fundamental mode with an analytic theory. In Sec. II, we introduce this theory which describes the dynamics of the two polarization modes and the inversion in a VCSEL. In particular, we focus on the validity of this theory for practical VCSEL's. In Secs. III and IV, expressions for the intensity noise spectra and for the polarization correlation function are derived, respectively. In Sec. V we present the experimental data; in the successive subsections we discuss the measured intensity and polarization-resolved noise spectra. From these we derive the correlation function and demonstrate its frequency dependence. Section VI gives a concluding discussion.

II. TWO-MODE THEORY FOR VCSEL'S

An appropriate theoretical framework for the intensity fluctuations of polarization modes and their correlation is formed by a set of Langevin rate equations for the two polarization modes and the inversion, i.e., we use a two-mode theory for a class-B laser. The advantage of such a two-mode theory is that it is a transparent starting point, formulated in terms of quantities that can be measured experimentally.

The standard theory to describe the polarization dynamics of quantum-well VCSEL's is the spin-flip model developed by San Miguel, Feng, and Moloney [8]. However, in its full generality this spin-flip theory allows only numerical solutions, permitting limited physical insight into the polarization dynamics. In this section we describe, by refining our earlier work [9], how one can obtain a simple two-mode description from the spin-flip theory.

The spin-flip theory [8] incorporates the vectorial nature of the optical polarization and models the conduction and heavy-hole valence band by four discrete spin levels, which interact as two pairs with the circular components of the optical field. Effectively this model has two inversion reservoirs corresponding to the average inversion and the spin-difference inversion.

The first approximation that we will apply is the adiabatic elimination of the spin-difference inversion [9–11]. This is allowed when both spin reservoirs are strongly coupled by spin scattering, which corresponds to a large value of Γ, being defined as the ratio of the decay rates of the spin-difference and average inversion. Experimental verification of this assumption has been demonstrated [9,12], yielding a relatively large value of $\Gamma \simeq 100$–800. After adiabatic elimination one obtains the following set of equations for the optical fields E_x and E_y and total inversion N:

$$\frac{dE_x}{dt} = \kappa(1-i\alpha)(N-1)E_x + i(\omega_{\mathrm{lin}}/2)E_x + (\gamma_{\parallel}/2)E_x - \frac{\kappa}{\Gamma}(1-i\alpha)[|E_y|^2 E_x + E_y^2 E_x^*] + F_{Ex}(t), \qquad (1a)$$

$$\frac{dE_y}{dt}=\kappa(1-i\alpha)(N-1)E_y-i(\omega_{\rm lin}/2)E_y-(\gamma_\parallel/2)E_y$$
$$-\frac{\kappa}{\Gamma}(1-i\alpha)[|E_x|^2E_y+E_x^2E_y^*]+F_{Ey}(t), \qquad (1b)$$

$$\frac{dN}{dt}=-\gamma(N-1-\mu)-\gamma(|E_x|^2+|E_y|^2)N$$
$$+\frac{\gamma}{\Gamma}[2|E_x|^2|E_y|^2-E_x^2(E_y^*)^2-(E_x^*)^2E_y^2]+F_N(t), \qquad (1c)$$

where 2κ is the intensity cavity-loss rate, $\omega_{\rm lin}$ is the linear birefringence, $\gamma_\parallel$ is the linear dichroism as projected onto the birefringence axes, α is the amplitude–phase-coupling factor [13], N is the total inversion (normalized with respect to lasing threshold), γ is the spontaneous inversion decay rate, and μ is the normalized pump parameter (at the lasing threshold $\mu=0$).

In Eqs. (1a) and (1b), the next-to-last terms (proportional to $1/\Gamma$) are remnants of the fast spin dynamics. The terms proportional to $|E_x|^2E_y$ and $|E_y|^2E_x$ correspond to the polarization dependence of the optical saturation (or nonlinear dichroism) and nonlinear birefringence. The terms with the complex conjugates correspond to a four-wave-mixing (FWM) effect, which is only observable in VCSEL's with small linear birefringence, where it shows up as a weak FWM peak in the optical spectrum [12].

The second approximation needed to obtain a two-mode theory involves a simplification in describing the optical field. In the general vectorial description of a polarized light field, one needs four variables, which we have chosen in our earlier work [9] as total intensity, optical phase, polarization angle ϕ, and ellipticity angle χ. In contrast, a two-mode theory requires only two variables, which can be chosen as the intensities of the two polarization modes x and y, or as the total intensity and the polarization angle.

The optical phase can always be eliminated, since it is not coupled to other variables due to time translation invariance. Although the steady-state polarization of a VCSEL is approximately linear, elimination of the ellipticity is not trivial. Difficulties arise in particular when polarization fluctuations become nonuniform in ϕ and χ, which is the case when nonlinear anisotropies are as strong or stronger than the linear anisotropies. Luckily, for almost every practical VCSEL, linear birefringence is the dominant anisotropy, which results in equal polarization fluctuations in ϕ and χ. In this case one optical degree of freedom can be eliminated by ''rotational averaging'' of the fluctuations [9]. The polarization can now be described with only one variable, being the polarization angle, remembering that the steady-state polarization is linear and that the fluctuations in the ellipticity can be directly derived from the fluctuations in the polarization angle. Of course one must check for practical cases whether the linear birefringence is indeed dominant. Recently we used a similar type of elimination to model stochastic polarization switching with a one-dimensional Kramers model [15]; the good agreement with the experiment in that case underlines the validity of such an approach for practical VCSEL's.

After the rotational averaging one obtains the following set of Langevin equations for the intensities I_x and I_y of the x- and y-polarized TEM_{00} modes and the inversion N:

$$\frac{dI_x}{dt}=2\kappa(N-1)I_x+\gamma_\parallel I_x-2\frac{\kappa}{\Gamma}I_xI_y+R_{\rm sp}\beta+F_x(t), \qquad (2a)$$

$$\frac{dI_y}{dt}=2\kappa(N-1)I_y-\gamma_\parallel I_y-2\frac{\kappa}{\Gamma}I_xI_y+R_{\rm sp}\beta+F_y(t), \qquad (2b)$$

$$\frac{dN}{dt}=-\gamma(N-1-\mu)-\gamma(I_x+I_y)N+2\frac{\gamma}{\Gamma}I_xI_y+F_N(t), \qquad (2c)$$

where F_x, F_y, and F_N are Langevin noise sources. Note that I_x and I_y are normalized with respect to the saturation intensity, so that $I=\beta n$ with n the number of photons in the laser cavity and β the spontaneous emission factor; finally, $R_{\rm sp}=2\kappa n_{\rm sp}$, where $n_{\rm sp}\geqslant 1$ quantifies the degree of inversion. Note that the rotational averaging corresponds to eliminating the FWM terms in Eqs. (1), i.e., the assumption of dominant linear birefringence reduces the number of polarization degrees of freedom from two to one, and also removes the FWM effect [9,12].

III. MODE-PARTITION NOISE

In this section we will derive expressions for the noise spectra of the total intensity and for the intensities in both polarization modes. In order to obtain these expressions, we linearize the Langevin equations [Eq. (2)] around the steady-state values $\overline{I_x}$, $\overline{I_y}$, and $\overline{N}\approx 1$. This results in the following set of Langevin difference equations for the fluctuations $\Delta I_x, \Delta I_y$ and ΔN:

$$\frac{d}{dt}\begin{pmatrix}\Delta I_x\\ \Delta I_y\\ \Delta N\end{pmatrix}=\begin{pmatrix}0 & -\frac{2\kappa}{\Gamma}\overline{I_x} & 2\kappa\overline{I_x}\\ -\frac{2\kappa}{\Gamma}\overline{I_y} & -2\gamma_\parallel-2\frac{\kappa}{\Gamma}(\overline{I_x}-\overline{I_y}) & 2\kappa\overline{I_y}\\ -\gamma+2\frac{\gamma}{\Gamma}\overline{I_y} & -\gamma+2\frac{\gamma}{\Gamma}\overline{I_x} & -\gamma(1+\overline{I_x}+\overline{I_y})\end{pmatrix}\cdot\begin{pmatrix}\Delta I_x\\ \Delta I_y\\ \Delta N\end{pmatrix}+\begin{pmatrix}F_x\\ F_y\\ F_N\end{pmatrix}, \qquad (3)$$

where the (small) loss in the dominant x mode was set to zero.

Next we solve these Langevin difference equations in the Fourier domain. As exact solution of the equations gives rather tedious expressions, we make two approximations. (i) The average intensity of the nonlasing mode ($\overline{I_y}$) is assumed to be much smaller than that of lasing mode ($\overline{I_x}$); this assumption is valid for practical VCSEL's (typically, we find $M \equiv \overline{I_y}/\overline{I_x} < 0.02$, as we will see below). Therefore, we will neglect terms proportional to $\overline{I_y}$ in Eq. (3). (ii) The contributions due to carrier noise is neglected, so that the Langevin noise sources are given by

$$\begin{aligned} \langle F_i(t) \rangle &= 0, \\ \langle F_x(t) F_x(t+\tau) \rangle &= 2R_{\rm sp}\beta \overline{I_x}\,\delta(\tau), \\ \langle F_y(t) F_y(t+\tau) \rangle &= 2R_{\rm sp}\beta \overline{I_y}\,\delta(\tau), \\ \langle F_x(t) F_y(t+\tau) \rangle &= 0, \end{aligned} \tag{4}$$

$$\langle F_N(t) F_N(t+\tau) \rangle = \langle F_N(t) F_x(t+\tau) \rangle = \langle F_N(t) F_y(t+\tau) \rangle = 0. \tag{5}$$

With these approximations, we find the following expressions for the noise spectra of the total intensity and the modal intensities:

$$\langle |I(\omega)|^2 \rangle = 2R_{\rm sp}\beta \overline{I_x} \frac{\omega^2 + 4\gamma_{\rm ro}^2}{(\omega^2 - \omega_{\rm ro}^2)^2 + 4\gamma_{\rm ro}^2 \omega^2}, \tag{6a}$$

$$\begin{aligned} \langle |I_x(\omega)|^2 \rangle = {} & 2R_{\rm sp}\beta \overline{I_x} \frac{\omega^2 + 4\gamma_{\rm ro}^2}{(\omega^2 - \omega_{\rm ro}^2)^2 + 4\gamma_{\rm ro}^2 \omega^2} \\ & + 2R_{\rm sp}\beta \overline{I_y} \frac{\omega_{\rm ro}^4}{[(\omega^2 - \omega_{\rm ro}^2)^2 + 4\gamma_{\rm ro}^2 \omega^2](\omega^2 + 4\gamma_0^2)}, \end{aligned} \tag{6b}$$

$$\langle |I_y(\omega)|^2 \rangle = 2R_{\rm sp}\beta \overline{I_y} \left(\frac{1}{\omega^2 + 4\gamma_0^2} \right), \tag{6c}$$

where $I = I_x + I_y$ is the total intensity, $\omega_{\rm ro} = (2\kappa\gamma \overline{I})^{1/2}$ the relaxation oscillation frequency, $\gamma_{\rm ro} = \gamma(1 + \overline{I})/2$ the relaxation oscillation damping rate, and γ_0 the dichroism, i.e., the damping of the polarization fluctuations. The dichroism $\gamma_0 = \gamma_\parallel + \gamma_{\rm non}$ consists of two parts [9]: a contribution due to the gain difference between the polarization modes, or projected linear dichroism ($\gamma_\parallel$); and a contribution due to cross saturation of the two polarization modes ($\gamma_{\rm non} = 2\kappa\mu/\Gamma$), resulting from the adiabatic elimination of the difference inversion [10,11].

The shape of the total intensity noise spectrum [Eq. (6a)] is determined by the relaxation oscillations [14]. Typical numbers for the relaxation oscillation frequency and damping, found for VCSEL's operating well above threshold, are in the range $\omega_{\rm ro}/2\pi = 2$–10 GHz and $\gamma_{\rm ro}/2\pi = 0.3$–$2$ GHz, respectively (see also Sec. V C). The intensity noise spectrum of the nonlasing mode y [Eq. (6c)] is due to mode-partition noise; it has a Lorentzian shape, centered at zero frequency, and a width of $2\gamma_0$. The mode-partition noise is concentrated at relatively low frequencies, because the dichroism in VCSEL's is typically $\gamma_0/2\pi = 0$–1 GHz [9,16].

The noise in the lasing mode x [Eq. 6b)] depends both on the relaxation oscillations and the mode partition fluctuations. The first term in Eq. (6b) is the same as the noise spectrum of the total intensity noise, and dominates at higher frequencies, being resonant around the relaxation oscillation frequency. The second term is important only at low frequencies, where it enhances the noise in the lasing mode as compared to the total intensity noise. For the typical values given above, the second term in Eq. (6b) dominates at lower frequencies, where it reduces to the mode-partition noise [Eq. (6c)].

At this stage, it is important to note that our approximations (i) and (ii) in this section resulted in a relatively simple *decoupled* description of the polarization fluctuations. By ''decoupled'' we mean that the fluctuations in the total output power are independent of the cavity anisotropies (dichroism and birefringence), which affect the polarization. The dichroism appears only in the noise spectra of the individual polarization modes. Linear birefringence was assumed to be sufficiently large, in order to perform the ''rotational averaging'' of the polarization fluctuations. A quantitative estimate of the remaining small effects of the polarization dynamics on the total intensity, in particular on intensity squeezing, are given in Ref. [17], where the present results are taken as a starting point.

Previously, we have derived an expression for the average modal ratio $M = \overline{I_y}/\overline{I_x}$, as $M = D/\gamma_0$ [9]. More spontaneous emission noise (D) makes the nonlasing mode (y) stronger, whereas more dichroism (γ_0) makes it weaker. In fact, the light in the nonlasing mode is ''chaotic'' or ''thermal,'' since integration of Eq. (6c) gives $\langle |\Delta I_y|^2 \rangle^{1/2} = \overline{I_y}$.

The amount of mode-partition noise will change in the same way as the average mode ratio. Weak dichroism will result in a strong nonlasing mode and large mode-partition noise. In this case, the noise level at low frequencies of the lasing mode will be only slightly higher than that of the nonlasing mode, and both noise levels will be very large as compared to the noise in the total output power. On the other hand, strong dichroism will damp the nonlasing mode and the mode partition noise of the nonlasing mode will disappear below the total intensity noise, while the noise level of the lasing mode will decrease toward that of the total intensity noise.

IV. MODAL CORRELATIONS

In this section we will derive analytic expressions for the correlation function in the case of decoupled polarization noise presented in Sec. III. The total intensity is given by the sum of intensities in the orthogonally linear polarized lasing and nonlasing mode, $I(t) = I_x(t) + I_y(t)$. The spectral density of the total intensity noise (or the intensity noise spectrum) is given, via the Wiener-Khinchin theorem, as the Fourier transform of the autocorrelation function,

$$S(\omega)=\langle|I(\omega)|^2\rangle=\int_{-\infty}^{\infty}\langle I(t)I(t+\tau)\rangle e^{i\omega\tau}d\tau$$
$$=S_x(\omega)+S_y(\omega)+S_{xy}(\omega)+S_{yx}(\omega), \tag{7}$$

where the individual noise spectra $S_{ij}(w)$ are given by similar integrals. The correlation function for the fluctuations in the lasing and nonlasing mode is defined by

$$C_{xy}(\omega)=\frac{\mathrm{Re}\{S_{xy}(\omega)\}}{\sqrt{S_x(\omega)\,S_y(\omega)}}, \tag{8}$$

where $\mathrm{Re}\{S_{xy}\}$ is the real part of the cross-spectral density.

To obtain this correlation from experimental data, it is more convenient to rewrite the correlation as

$$C_{xy}(\omega)=\frac{S(\omega)-S_x(\omega)-S_y(\omega)}{2\sqrt{S_x(\omega)\,S_y(\omega)}}. \tag{9}$$

The correlation is now expressed as a normalized balance between the total intensity noise and the fluctuations of both polarization modes.

For decoupled fluctuations, i.e., $\langle\Delta I(t_1)\Delta I_y(t_2)\rangle=0$, a case which naturally occurs when the power in the nonlasing mode is much smaller than that in the lasing mode ($\overline{I_y}\ll\overline{I_x}$), the correlation function can be reduced to

$$C_{xy}(\omega)=\frac{-1}{\sqrt{1+S(\omega)/S_y(\omega)}}. \tag{10}$$

Comparison of the measured correlation analyzed according to Eq. (9) or Eq. (10) can demonstrate whether polarization fluctuations are indeed decoupled from total intensity fluctuations.

A theoretical expression for the correlation can be obtained by substituting the noise spectra of Eqs. (6) into Eq. (9), which gives a rather cumbersome result. Since in most experiments the correlation is investigated at low (MHz) frequencies, we will focus on the low-frequency limit

$$C_{xy}(\omega=0)=\frac{-1}{\sqrt{1+\left(4\dfrac{\gamma_0\gamma_{\mathrm{ro}}}{\omega_{\mathrm{ro}}^2}\right)^2\Big/M}}, \tag{11}$$

where $M=\overline{I_y}/\overline{I_x}$ is the mode ratio. Equation (11) shows that for smaller dichroism, which corresponds to a relatively strong nonlasing mode and thus more mode-partition noise, the polarization fluctuations become perfectly anticorrelated. The degree of anticorrelation is a measure of the amount of mode-partition noise, as the correlation results from a balance between total intensity noise and polarization noise of the modes [see Eq. (9)]. Increasing the damping and/or decreasing the frequency of the relaxation oscillations leads to an increase of the low-frequency noise in the total output power and lasing mode. This reduces the degree of anticorrelation [see Eqs. (9) and (10)].

A demonstration of the frequency dependence of the correlation can be given by an expansion for $\omega\ll\omega_{\mathrm{ro}}$,

$$C_{xy}(\omega\ll\omega_{\mathrm{ro}})\approx-1+\frac{8}{M}\left(\frac{\gamma_{\mathrm{ro}}\gamma_0}{\omega_{\mathrm{ro}}^2}\right)^2[1+\omega^2/(4\gamma_0^2)]$$
$$\times[1+\omega^2/(4\gamma_{\mathrm{ro}}^2)], \tag{12}$$

where we have used $\gamma_{\mathrm{ro}}\ll\omega_{\mathrm{ro}}$. The expansion of the square root in Eq. (10) is only valid when $C_{xy}(\omega\approx0)\leqslant-0.8$. Equation (12) shows that at higher frequencies the degree of anticorrelation decreases, because the amount of Lorentzian mode-partition noise decreases, whereas the total intensity noise increases.

V. EXPERIMENTAL RESULTS

In this section, we compare results from experiments, performed on a VCSEL oscillating in the two TEM_{00} polarization modes, with the theoretical results presented in Secs. II–IV. Specifically, in Sec. V A we discuss measured intensity and polarization-resolved noise spectra. In Sec. V B we check whether the polarization fluctuations are decoupled from the total intensity noise. In Sec. V C, we verify specific results for the correlation based upon the developed two-mode theory, these being the dependence of the correlation on the dichroism and relaxation oscillations and on the frequency.

A. Intensity and polarization-resolved noise spectra

For the experiments we have used a batch of about 50 proton-implanted VCSEL's [18]. The lasers consist of 1-λ cavity with three 8-nm-thick quantum wells. The VCSEL's have a threshold injection current around 5 mA, while higher-order spatial modes start lasing above 10 mA. We have limited ourselves to the regime of fundamental transverse mode operation.

Almost every individual device fulfilled the requirements for a two-mode description discussed in Sec. II; specifically, the condition for adiabatic elimination of the difference inversion was previously shown to be valid for this particular set of VCSEL's [9], and more than 90% of the lasers had a sufficiently large birefringence to allow the ''rotational averaging'' of the state of polarization.

We concentrated on the devices that exhibited a polarization switch. As the polarization stability of these switching devices changes a great deal as a function of current, they allow for a rather accurate comparison with theory. The requirement that the VCSEL should exhibit a polarization switch was quite a strong one for the batch under study and decimated the amount of suitable VCSEL's to six. Since a detailed study showed the polarization-resolved intensity noise of the remaining devices to be similar, we will give the results for one laser only.

The selected VCSEL had a birefringence of 11 GHz and a polarization switch at a current of 8.2 mA, centered in its studied fundamental transverse mode regime between 6.0 and 9.5 mA. The threshold of this device was 5.0 mA, and higher-order modes appeared at a current of 10.0 mA.

To measure the intensity noise of the lasing and nonlasing polarization mode, the emitted light was passed through a

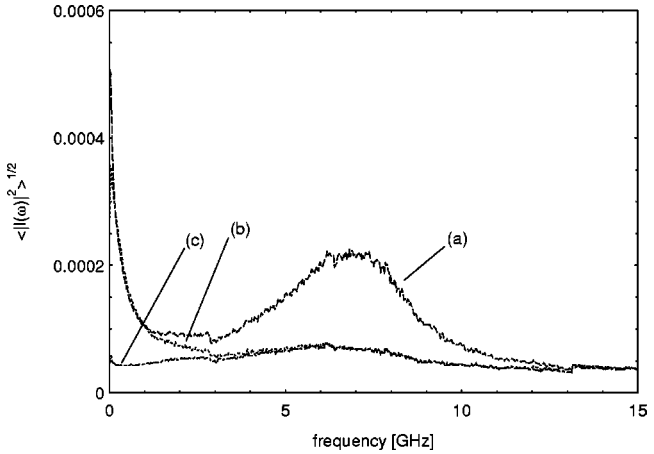

FIG. 1. Broadband intensity noise of the lasing mode (a) and the nonlasing mode (b) measured with a 6-GHz photoreceiver. The lowest trace is the background noise (c). The spectrum of the lasing mode contains mode-partition noise and fluctuations due to relaxation oscillations, whereas the spectrum of the nonlasing mode only contains mode-partition noise.

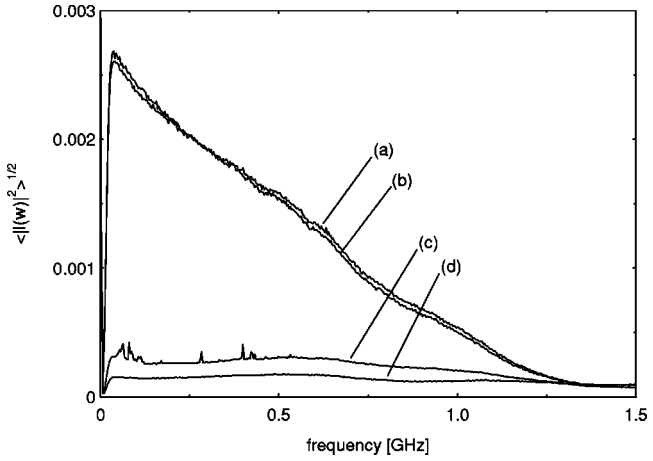

FIG. 2. Intensity noise measurements with a 1-GHz photo receiver of the lasing mode (a), the nonlasing mode (b), the total intensity (c), and the no-light reference (d). The polarization mode-partition noise clearly dominates over the total intensity noise.

$\lambda/4$ wave plate, a $\lambda/2$ wave plate, and an optical Faraday isolator. The polarization-resolved intensity noise was first measured with a 6-GHz photoreceiver (New Focus 1534). In Fig. 1 the intensity noise of the lasing and nonlasing polarization mode is shown as traces (a) and (b), respectively, at a laser current of 7.5 mA. At low frequencies the intensity noise of the nonlasing and lasing mode is relatively high. The amount of low-frequency noise decreased when a combination of the two polarization modes was selected. A more detailed inspection of the mode-partition noise showed that the spectra were Lorentzian, having the same width for the lasing mode and the nonlasing mode. At higher frequencies the relaxation oscillations are visible in the spectrum of the lasing mode, but not in the (much weaker) nonlasing mode. The fits of the measured noise spectra were in qualitative good agreement with the theoretical expressions (6b) and (6c).

Next we measured the total intensity noise (not shown): it exhibited only the relaxation oscillation peak, but was somewhat noisy due to unintentional optical feedback, that existed after the necessary removal of the optical isolator. The 6-GHz detector is a fiber-coupled detector, in order to facilitate alignment, which made feedback from the fiber ends hard to avoid. Better measurements of the total intensity noise were done with a slower 1-GHz detector (New Focus 1601), which was aligned at a small angle to prevent feedback. In Fig. 2 four noise traces [(a)–(d)] are shown at laser current of 7.75 mA; traces (a) and (b) are from the lasing mode and nonlasing mode, respectively, and traces (c) and (d) are the total intensity noise and a reference measurement in the absence of light, respectively. Figure 2 demonstrates that the mode-partition noise in polarization-resolved spectra is much larger than the total intensity noise.

To measure the intensity noise more accurately at low frequencies, we used a detector with a home-built preamplifier with a bandwidth of 40 MHz. The noise level of this detector was calibrated with a white-light source, and was found to be shot noise limited above 0.2 mW (in the measurements, the total output power of the VCSEL was always above 1 mW). In Fig. 3 we show the noise spectra of the polarization modes and of the total output power, measured with the 40-MHz detector at a laser current of 7.75 mA. The lowest trace (d) displays the background noise. The absolute level of the total intensity noise [trace (c)] around 20 MHz was -148 dB/Hz, which was 3.7 dB above the shot-noise level. Note that the low-frequency measurements with the 40-MHz detector zoom in on the top of Lorentzian shaped mode-partition noise in Figs. 1 and 2. The frequency dependence of the noise traces is due to the detector response; after compensation for this, the polarization-resolved intensity noise [traces (a) and (b)] was found to be approximately flat up to 50 MHz (not shown), as expected from the other measurements. The intensity noise of the lasing mode was slightly higher than that of the nonlasing mode, again as expected from theory.

B. Decoupled fluctuations

In this section we will check whether or not intensity and polarization fluctuations are decoupled. This is done by measuring the correlation and analyzing it according to Eq. (9) and to Eq. (10) over the full range of fundamental transverse

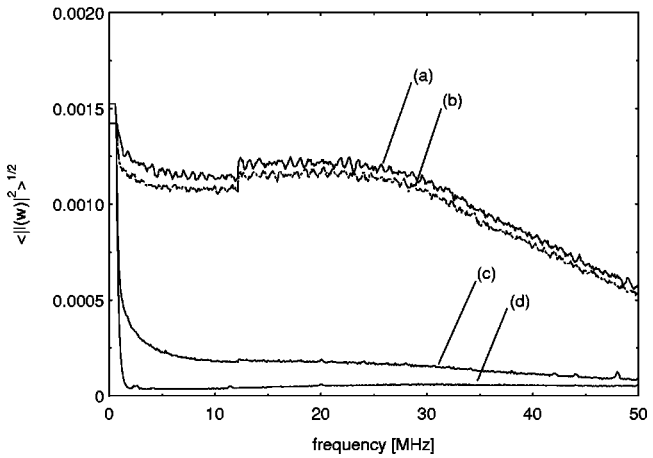

FIG. 3. Intensity noise measurements with a 40-MHz photo receiver of the lasing mode (a), the nonlasing mode (b), the total intensity (c), and the no-light reference (d).

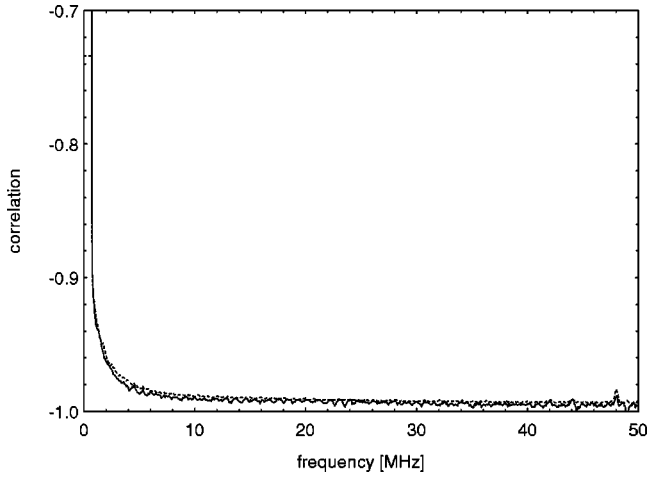

FIG. 4. Correlation C_{xy} as a function of frequency calculated from measurements in Fig. 3, using Eqs. (9) (solid curve) and (10) (dashed curve).

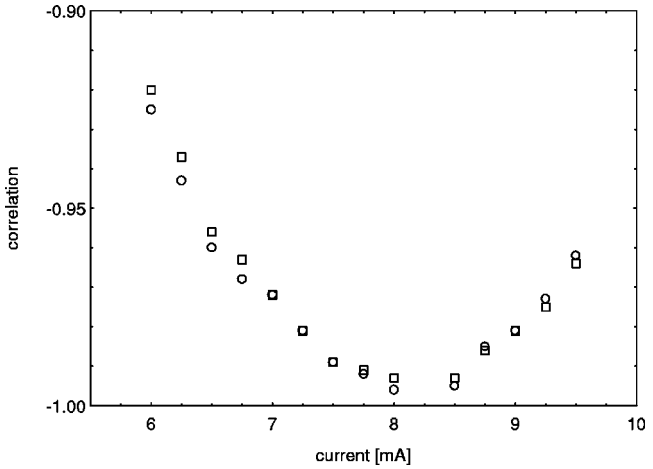

FIG. 5. Correlation at 20 MHz as a function of the laser current. The circles show the correlation calculated from Eq. (9). The squares show the correlation calculated from Eq. (10), where it was assumed that the intensity and polarization fluctuations are decoupled.

mode operation. Before we make this analysis, we will first study the mode partition noise as a function of laser current, starting with the 40-MHz detector.

Increasing the current toward the polarization switch ($i_{\mathrm{switch}} \approx 8.2$ mA), we observed an increase in the noise levels of the lasing mode and nonlasing mode, whereas after the switch the noise levels decrease. The noise level of the lasing mode was always slightly higher than that of the nonlasing mode. The reason that the noise levels of the polarization modes reach a maximum at the hop is that the mode-partition noise is strongest where the polarization competition is also strongest, being around the switching current.

By monitoring the mode-partition noise with the 6-GHz detector, we found that the mode partition became stronger toward the hop, while the width of the Lorentzian ($2\gamma_0$) decreased. This explains the observed increase of the noise at MHz frequencies, since less damping (dichroism) results in a stronger nonlasing mode and more polarization noise concentrated around lower frequencies. After the hop the Lorentzian noise spectrum becomes weaker and broader. A more detailed discussion of the dichroism as a function of current will be given in Sec. V C.

The mode-partition dynamics discussed above had no observable effect on the total intensity noise. In fact it was impossible to distinguish between VCSEL's with or without a polarization hop by observing only the total intensity noise. This confirms the decoupled polarization-fluctuation framework that we introduced in Sec. III.

To determine the correlation of the polarization fluctuations, measured with the 40-MHz detector, we first used Eq. (9). Since the correlation is proportional to the difference in total intensity noise and polarization-resolved intensity noise, it is obvious from the data [Fig. 3] that the fluctuations are anticorrelated because the intensity noise in each of the two polarization modes is almost equal and relatively large as compared to the total intensity noise. The correlation for low frequencies, as derived from the measurements in Fig. 3 using Eq. (9), is shown in Fig. 4 (solid curve); in the transformation of Fig. 3 into Fig 4 we have compensated for the loss due to the polarization projection and subtracted the background noise quadratically. The fluctuations in the two polarization modes are indeed found to be almost completely anticorrelated.

To check whether or not the polarization noise is decoupled from the intensity noise, we also calculated the correlation from the measured noise spectra of the nonlasing polarization mode and the total output power according to Eq. (10). This result is depicted as the dashed curve in Fig. 4. As it agrees with the correlation found from the analysis based upon Eq. (9), this proves again the validity of a decoupled description.

As a next step we measured the total intensity noise and the intensity noise in both polarizations as a function of current, to calculate the correlation as before. The result is shown in Fig. 5, where the correlation at 20 MHz is plotted as a function of laser current; circular and square data points show the correlation deduced using Eq. (9) and Eq. (10), respectively. From the good agreement between the two methods of analysis, we conclude that the polarization fluctuations are decoupled from the total intensity noise over the full range of TEM_{00} operation.

When the current is increased toward the hop ($i_{\mathrm{switch}} \approx 8.2$ mA) the degree of anticorrelation increases because the mode-partition noise becomes larger, whereas the total intensity noise is almost constant. Around the hop the modal fluctuations were found to be almost exactly anticorrelated, as $C_{xy} = -0.997(2)$. After the hop, where the mode-partition noise becomes again smaller due to larger damping (dichroism), the degree of anticorrelation decreases accordingly.

C. Correlation and its frequency dependence

So far, we have analyzed the correlation directly from its definition, as a normalized balance between total intensity fluctuations and the intensity fluctuations of the polarization modes [Eq. (9)]. We will now verify the theoretical predictions for the correlation [Eqs. (11) and (12)], which are based on the two-mode theory developed in Sec. II. In order to do this we will first independently determine the parameters ω_{ro}, γ_{ro}, γ_0, and M.

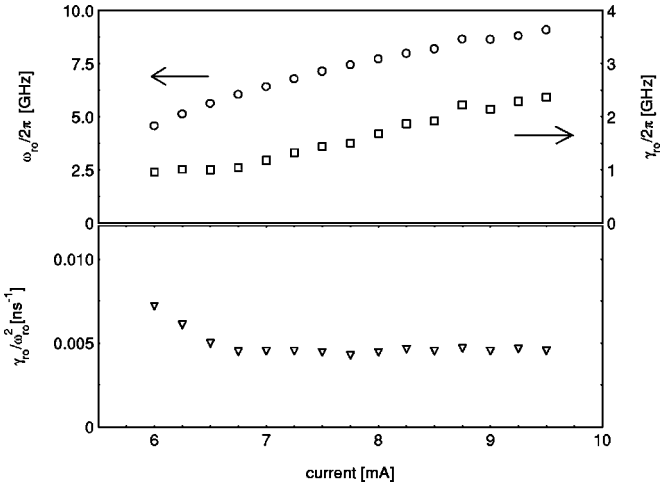

FIG. 6. Current dependence of the relaxation oscillation frequency ω_{ro} and damping rate γ_{ro} (upper graph) and the ratio $\gamma_{ro}/\omega_{ro}^2$ (lower graph).

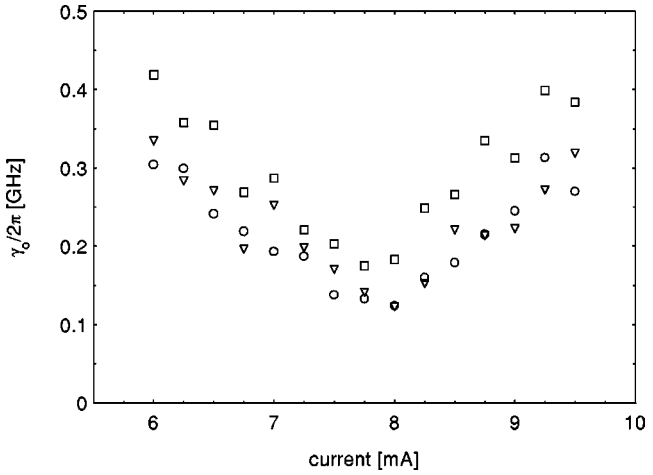

FIG. 7. Dichroism as a function of laser current. The dichroism was determined from optical spectra with a Fabry-Pérot (triangles), from mode-partition noise spectra (circles), and from beat spectra between the polarization modes (squares).

The relaxation oscillations were investigated by fitting the high-frequency intensity noise of the lasing mode to Eq. (6b). The upper box of Fig. 6 shows the relaxation oscillation frequency (ω_{ro}) and damping (γ_{ro}) determined as a function of current. The relaxation oscillations were measured with the 6-GHz detector. Since for higher currents the relaxation oscillations frequency approaches almost 10 GHz, the response of the detector was calibrated and corrected for, which made measurements possible up to 12 GHz.

The important parameter for the correlation is the ratio $\gamma_{ro}/\omega_{ro}^2$ [Eq. (11)]. The lower box of Fig. 6 shows that this ratio is almost constant as a function of current, being 5×10^{-3} ns^{-1}; near threshold the ratio increases somewhat.

The effective dichroism (γ_0), which is the difference in gain between the lasing and nonlasing mode, can be measured in three different ways. The first method, as discussed in Sec. V A, is to measure the width $2\gamma_0$ of the Lorentzian-shaped mode-partition intensity noise spectrum. In the second method, the dichroism γ_0 is obtained from the optical spectrum, as the difference in width [half width at half maximum (HWHM)] of the Lorentzian-shaped peaks of the lasing mode and the nonlasing mode. The third method is to pass the VCSEL light through a polarizer oriented at 45°, which transmits 50% of the lasing mode and the nonlasing mode. The intensity noise spectrum after this polarization projection contains a beat, with a resonance frequency equal to the birefringence, or frequency difference of the lasing and nonlasing mode. The width (HWHM) of this beat is equal to the effective dichroism. The dichroism as function of current is plotted in Fig. 7. All three methods reveal that the dichroism becomes smaller toward the hop. The three methods are in reasonable agreement; there is no obvious cause for the remaining differences. Note that after the switch the dichroism (i.e., the polarization stability) increases again. Figure 7 demonstrates that the current dependence of the dichroism, which results in a minimum at a certain current, is the actual origin of the polarization switch at that current. Recently we have shown experimentally that the remaining dichroism at the polarization hop is in fact the nonlinear dichroism ($2\kappa\mu/\Gamma$), i.e., the polarization-dependent cross saturation [9,15]. The physical mechanism of the current dependence of the linear dichroism is still somewhat of a mystery. However, we have observed that this current dependence of the dichroism is roughly the same in almost every VCSEL in this batch; this includes VCSEL's with small or large positive birefringence and even negative birefringence (see also Ref. [9]).

The average intensity ratio of the nonlasing mode and lasing mode (M) was determined from polarization-resolved power measurements and Fabry-Pérot spectra. From power measurements we obtained values of M ranging between 8×10^{-3} and 1.7×10^{-2}, whereas the mode ratio determined from areas under the peaks in the optical spectrum resulted in values between 5×10^{-3} and 1.7×10^{-2}. For both methods the mode ratio was maximum (1.7×10^{-2}) near the polarization switch.

As mentioned in Sec. III, one expects the mode ratio M to be approximately equal to the spontaneous emission noise strength D divided by the effective dichroism γ_0 [9]. Larger dichroism increases the polarization stability and thus the mode ratio, whereas more noise makes the nonlasing mode stronger and decreases the mode ratio.

Comparing the measured mode ratios with the measured variations in the dichroism γ_0, we found somewhat better agreement for the spectral measurements of the mode ratios. We attribute the difference to very weak spontaneous emission in many very heavily damped higher-order transverse modes. This was confirmed by the observation of a flat offset in the Fabry-Pérot spectrum of the nonlasing mode. In order to put this into the proper perspective, we emphasize that it was not possible to identify individual higher-order modes with a grating-based spectrum analyzer at intensities above 10^{-3} times that of the nonlasing mode. For our calculation of the correlation function [Eq. (11)], we will use the mode ratios from the power measurements, since these are more closely related to the direct measurement of the correlation.

The correlation of polarization fluctuations as calculated from the measured relaxation oscillation frequency and width, the dichroism measured with the Fabry-Pérot cavity, and the mode ratio is shown in Fig. 8 (squares). Figure 8 demonstrates that the correlation ''calculated'' from Eq. (11) is in quantitative agreement with the directly measured-

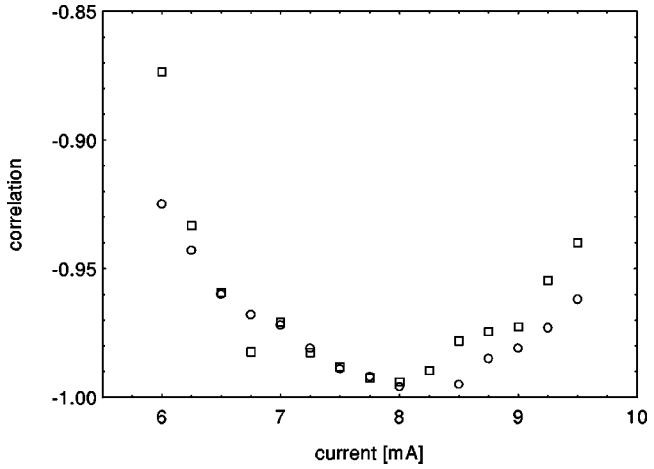

FIG. 8. Correlation at 20 MHz as a function of the laser current. The circles show the directly measured correlation function (the same circular points as in Fig. 5). The squares show the correlation calculated from measurements of the relaxation oscillations, dichroism, and mode ratio using Eq. (11).

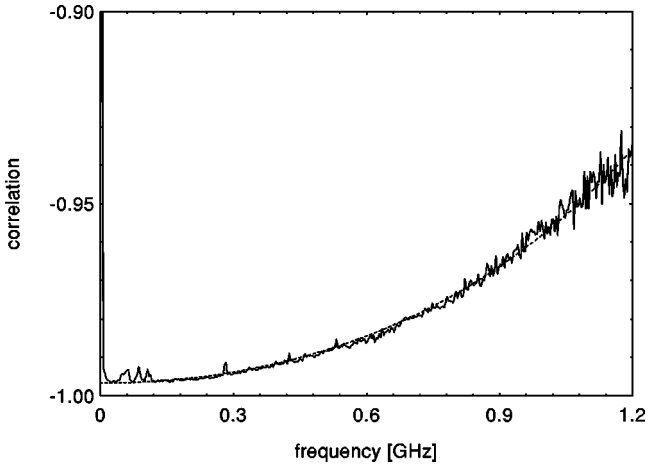

FIG. 9. Correlation C_{xy} as a function of frequency determined from measurements in Fig. 2 with Eq. (9) (solid curve). The dashed curve is a fit to Eq. (12).

correlation from the noise spectra based upon Eq. (9) (circles).

An experimental demonstration of the frequency dependence of the correlation is given in Fig. 9 (solid curve), where the correlation was determined from the noise in the total intensity and the individual polarization modes measured with the 1-GHz detector. We note that the detector responsivity divides out in the calculation of $C_{xy}(\omega)$. At higher frequencies the degree of anticorrelation drops, since the Lorentzian-shaped mode-partition noise spectrum decreases and approaches the total intensity noise spectrum. Fitting the measured correlation with Eq. (12) (the dashed curve in Fig. 9) resulted in values of $\gamma_0/2\pi=0.16$ GHz and $\gamma_{ro}/2\pi=1.0$ GHz for the damping of the polarization fluctuations and of the relaxation oscillations, respectively. These values are in reasonable agreement with direct measurements, which yield $\gamma_0/2\pi=0.15$ GHz and $\gamma_{ro}/2\pi=1.5$ GHz, respectively.

VI. CONCLUSION

In conclusion, we have presented a two-mode theory valid for the two polarization modes of a practical VCSEL. By ''practical'' VCSEL's we mean VCSEL's that have dominant linear birefringence, strongly coupled spin reservoirs, and a nonlasing mode that is much weaker than the lasing mode. We have derived noise spectra for the total output power and for the intensities of the separate polarization modes and predicted that for practical VCSEL's, polarization fluctuations are *decoupled* from the total intensity noise. We have shown quantitatively how the correlation function C_{xy} is expected to depend on the dichroism and relaxation oscillations. Furthermore we have demonstrated that the correlation function is frequency dependent.

The experimental results confirm this remarkably simple description of decoupled polarization dynamics. Specifically, (i) we have observed no effect on the total intensity noise from the polarization dynamics; (ii) we have checked polarization fluctuations to be decoupled from the intensity fluctuations by analyzing the correlation with Eq. (9) and with Eq. (10); (iii) the measured correlation was found to depend on the dichroism and relaxation oscillations, as was expected from theoretical predictions; and (iv) we have also experimentally demonstrated the frequency dependence of the correlation function.

Furthermore we have demonstrated, by three independent methods, that the dichroism has a minimum at the polarization switch (Fig. 7). A physical explanation of this current dependence of the linear dichroism, i.e., the actual origin of the polarization switch, is still under investigation.

The validity of a decoupled description of the polarization noise has interesting consequences for the generation of squeezed light in a single-transverse-mode VCSEL. Since we have observed the polarization fluctuations to be decoupled from the total intensity noise, one expects that polarization dynamics cannot deteriorate squeezing. We have addressed these aspects in detail elsewhere [17].

ACKNOWLEDGMENTS

We acknowledge support from the European Union under ESPRIT Project No. 20029 (ACQUIRE) and from TMR Network No. ERB4061 PL951021 (Microlasers and Cavity QED). This work is part of the program of the Foundation for Fundamental Research of Matter (FOM).

[1] K.D. Choquette, R.P. Schneider, Jr., K.L. Lear, and R.E. Leibenguth, IEEE J. Sel. Top. Quantum Electron. **1**, 661 (1995).

[2] C.J. Chang-Hasnain, J.P. Harbison, L.T. Florez, and N.G. Stoffel, Electron. Lett. **27**, 163 (1991).

[3] J. Martin-Regalado, J.L.A. Chilla, J.J. Rocca, and P. Brusenbach, Appl. Phys. Lett. **70**, 3350 (1997).

[4] A.K. Jansen van Doorn, M.P. van Exter, A.M. van der Lee, and J.P. Woerdman, Phys. Rev. A **55**, 1473 (1997).

[5] E. Goobar, J.W. Scott, B. Thibeault, G. Robinson, Y. Akulova,

and L.A. Goldren, Appl. Phys. Lett. **67**, 3697 (1995).
[6] D.C. Kilper, P.A. Roos, J.L. Carlsten, and K.L. Lear, Phys. Rev. A **55**, R3323 (1997)
[7] J.L. Vey and W. Elsasser, Opt. Lett. **23**, 721 (1998).
[8] M. San Miguel, Q. Feng, and J.V. Moloney, Phys. Rev. A **52**, 1728 (1995).
[9] M.P. van Exter, M.B. Willemsen, and J.P. Woerdman, Phys. Rev. A **58**, 4191 (1998).
[10] H.F. Hofmann and O. Hess, Quantum Semiclassic. Opt. **10**, 87 (1998).
[11] M.P. van Exter, R.F.M. Hendriks, and J.P. Woerdman, Phys. Rev. A **57**, 2080 (1998).
[12] M.P. van Exter, A. Al-Remawi, and J.P. Woerdman, Phys. Rev. Lett. **80**, 4875 (1998).
[13] C.H. Henry, IEEE J. Quantum Electron. **18**, 259 (1982).
[14] M.C. Tatham, I.F. Lealman, C.P. Seltzer, L.D. Westbrook, and D.M. Cooper, IEEE J. Quantum Electron. **28**, 408 (1992).
[15] M.B. Willemsen, M.U.F. Khalid, M.P. van Exter, and J.P. Woerdman, Phys. Rev. Lett. **82**, 4815 (1999).
[16] M.P. van Exter, M.B. Willemsen, and J.P. Woerdman, Appl. Phys. Lett. **74**, 2274 (1999).
[17] M. P. van Exter, M. B. Willemsen, and J. P. Woerdman (unpublished).
[18] Vixel Corporation, 325 Interlocken Parkway, Broomfield, CO 80021, model PRI-LA-S-850-1x8-3S.